

Supporting information

**New Type of Tin(IV) complex based Turn-on Fluorescent Chemosensor for Fluoride ion Recognition: Elucidating the Effect of Molecular Structure on Sensing Property**

*Andrew Wu,<sup>1</sup> Patrick C. Hillesheim,<sup>2</sup> Peter N. Nelson,<sup>3</sup> Matthias Zeller,<sup>4</sup> Gia Carignan,<sup>5</sup> Jing Li,<sup>5</sup> and Daniel W. Ki,<sup>1\*</sup>*

<sup>1</sup>School of Natural Sciences and Mathematics, Stockton University, New Jersey, 08205, United States

<sup>2</sup>Department of Chemistry and Physics, Ave Maria University, Ave Maria, Florida, 34142, United States

<sup>3</sup>Department of Chemistry, The University of the West Indies Mona, Jamaica

<sup>4</sup>Department of Chemistry, Purdue University, West Lafayette, Indiana, 47907, United States

<sup>5</sup>Department of Chemistry and Chemical Biology, Rutgers University, Piscataway, New Jersey 08854, United States

Email: [Daniel.Ki@stockton.edu](mailto:Daniel.Ki@stockton.edu)

Table of Contents

Figure S1. Experimentally collected and the simulated PXRD for compounds **1-3**

Table S1. Crystallographic details and information for compounds **2** and **3**

Figure S2. Depictions of the hydrogen interactions with the halide moieties within complexes

Figure S3. Depictions of the  $\pi$  stacking interactions with the halide moieties within complexes

Figure S4. Calculated MO surfaces for complex **2** (a) and complex **3** (b)

Figure S5. FL emission spectrum of complex **3** in MeCN solution and crystalline solid state

Figure S6. Benesi-Hildebrand plot of complex **1**

Figure S7. Job's plot of complex **1**

Figure S8. Fluorescence emission response of complex **1** against concentrations of fluoride ions

Figure S9. Fluorescence titration spectra(a) and UV-vis titration spectra (b) of complex **2**

Figure S10. UV-Vis spectral changes upon the addition of tetrabutylammonium fluoride ( $1.0 \times 10^{-3}$  M in MeCN) in  $\text{Snq}_2\text{Cl}_2$  ( $1.0 \times 10^{-5}$  M in MeCN).

Figure S11. Benesi-Hildebrand plot of  $\text{Snq}_2\text{Cl}_2$

Figure S12. Job's plot for complex  **$\text{Snq}_2\text{Cl}_2$** - fluoride interactions

Figure S13. Emission intensity changes of  $\text{Snq}_2\text{Cl}_2$  in the presence of anions (2 equiv) in MeCN

Figure S14. Optimized structure of  $\text{Snq}_2\text{Cl}_2$ ,  $\text{Sn}(\text{meq})_2\text{Cl}_2$ , and  $\text{Sn}(\text{dmqo})_2\text{Cl}_2$

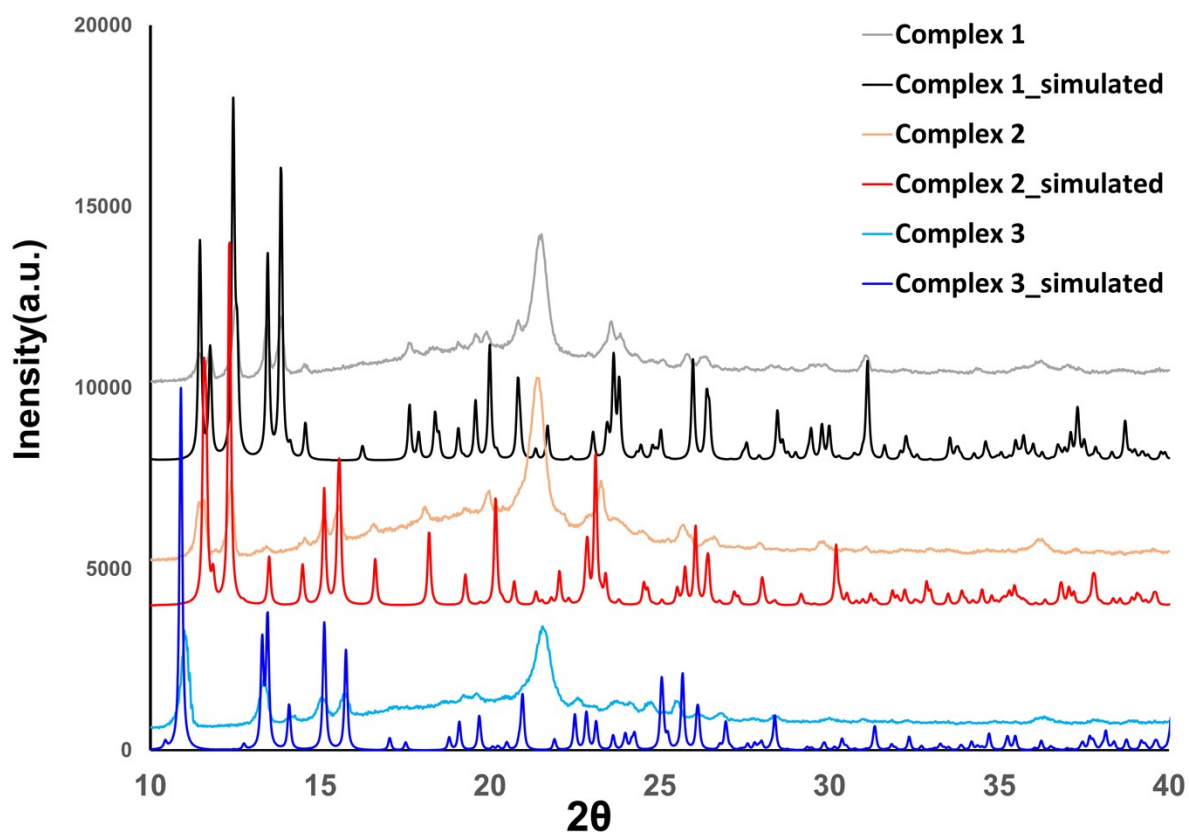


Fig. S1 Simulated and experimentally collected PXRD patterns for compounds **1-3**

	Complex 2	Complex 3
Crystal data		
Chemical formula	C <sub>20</sub> H <sub>16</sub> Cl <sub>0.67</sub> F <sub>1.33</sub> N <sub>2</sub> O <sub>2</sub> Sn	C <sub>20</sub> H <sub>16</sub> F <sub>2</sub> N <sub>2</sub> O <sub>2</sub> Sn
<i>M<sub>r</sub></i>	484.12	473.04
Crystal system, space group	Monoclinic, <i>P2<sub>1</sub>/c</i>	Triclinic, <i>P1</i>
Temperature (K)	150	150
<i>a</i> , <i>b</i> , <i>c</i> (Å)	13.7385 (4), 8.5689 (3), 15.9194 (5)	7.7896 (5), 9.5538 (5), 13.4786 (8)
$\alpha$ , $\beta$ , $\gamma$ (°)	107.426 (1)	70.205 (3), 75.540 (3), 66.973 (3)
<i>V</i> (Å <sup>3</sup> )	1788.08 (10)	860.61 (9)
<i>Z</i>	4	2
Radiation type	Cu <i>K</i> $\alpha$	Mo <i>K</i> $\alpha$
$\mu$ (mm <sup>-1</sup> )	12.58	1.52
Crystal size (mm)	0.21 × 0.16 × 0.12	0.05 × 0.04 × 0.03
Data collection		
Diffractometer	Bruker AXS D8 Quest	Bruker AXS D8 Quest
Absorption correction	Multi-scan <i>SADABS</i> 2016/2: Krause, L., Herbst-Irmer, R., Sheldrick G.M. & Stalke D., <i>J. Appl. Cryst.</i> 48 (2015) 3-10	Multi-scan <i>SADABS</i> 2016/2: Krause, L., Herbst-Irmer, R., Sheldrick G.M. & Stalke D., <i>J. Appl. Cryst.</i> 48 (2015) 3-10
<i>T<sub>min</sub></i> , <i>T<sub>max</sub></i>	0.593, 0.754	0.684, 0.747
No. of measured, independent and observed [ <i>I</i> > 2 $\sigma$ ( <i>I</i> )] reflections	52440, 3870, 3618	44029, 6561, 5697
<i>R<sub>int</sub></i>	0.063	0.052
( <i>sin</i> $\theta$ / $\lambda$ ) <sub>max</sub> (Å <sup>-1</sup> )	0.639	0.771
Refinement		
<i>R</i> [ <i>F</i> <sup>2</sup> > 2 $\sigma$ ( <i>F</i> <sup>2</sup> )], <i>wR</i> ( <i>F</i> <sup>2</sup> ), <i>S</i>	0.041, 0.091, 1.20	0.030, 0.068, 1.07
No. of reflections	3870	6561
No. of parameters	256	246
No. of restraints	7	0
H-atom treatment	H-atom parameters constrained	H-atom parameters constrained
$\Delta\rho_{max}$ , $\Delta\rho_{min}$ (e Å <sup>-3</sup> )	0.82, -1.43	1.57, -0.88

Table S1. Crystallographic details and information for compounds **2** and **3**

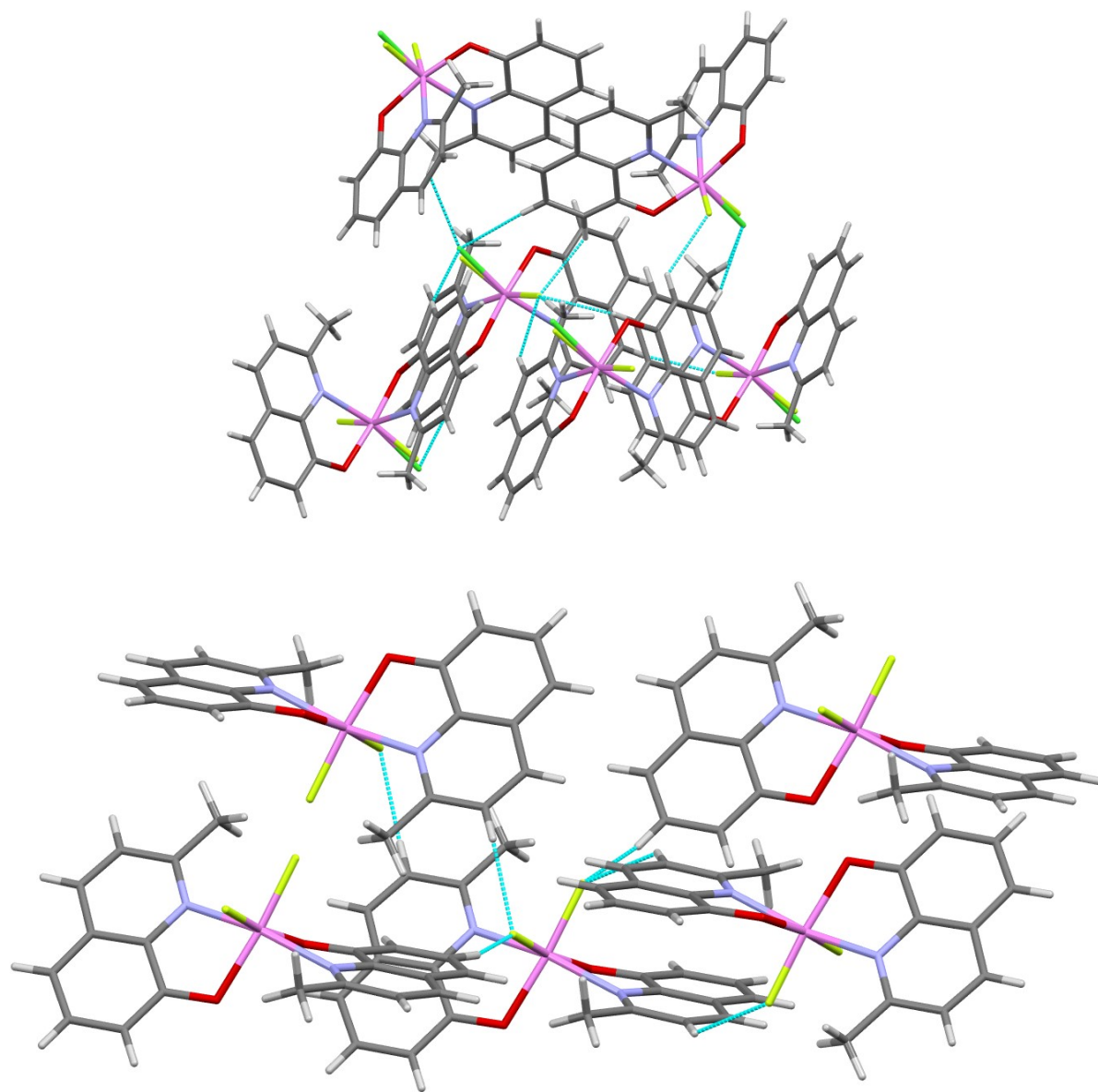


Figure S2. Depictions of the hydrogen interactions with the halide moieties within complex **2** (top) and complex **3** (bottom). Interactions are shown as blue dotted lines.

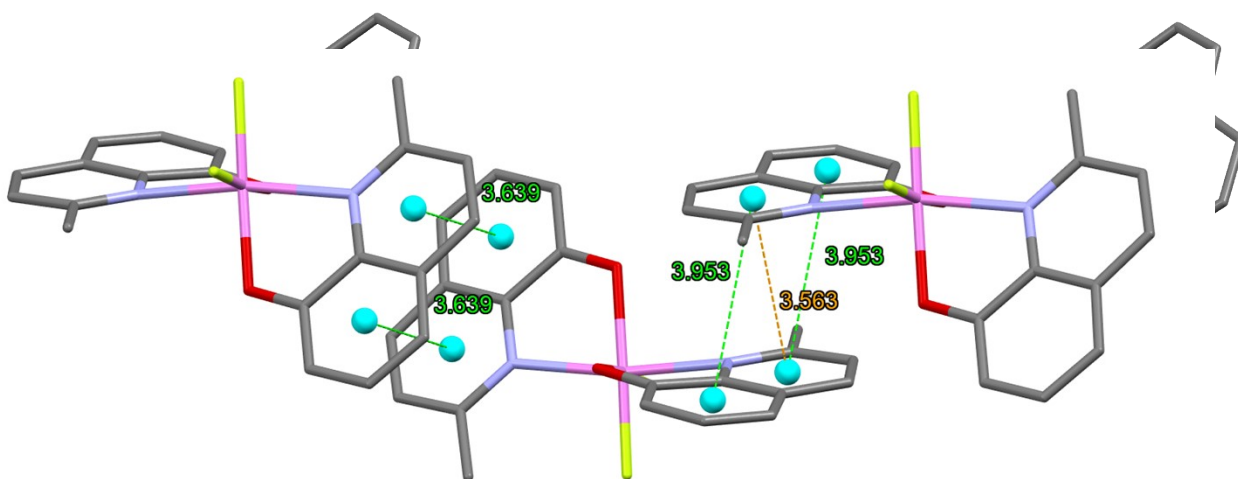


Figure S3. Depictions of the  $\pi$  stacking interactions with the halide moieties within complex **2** (top) and complex **3** (bottom).

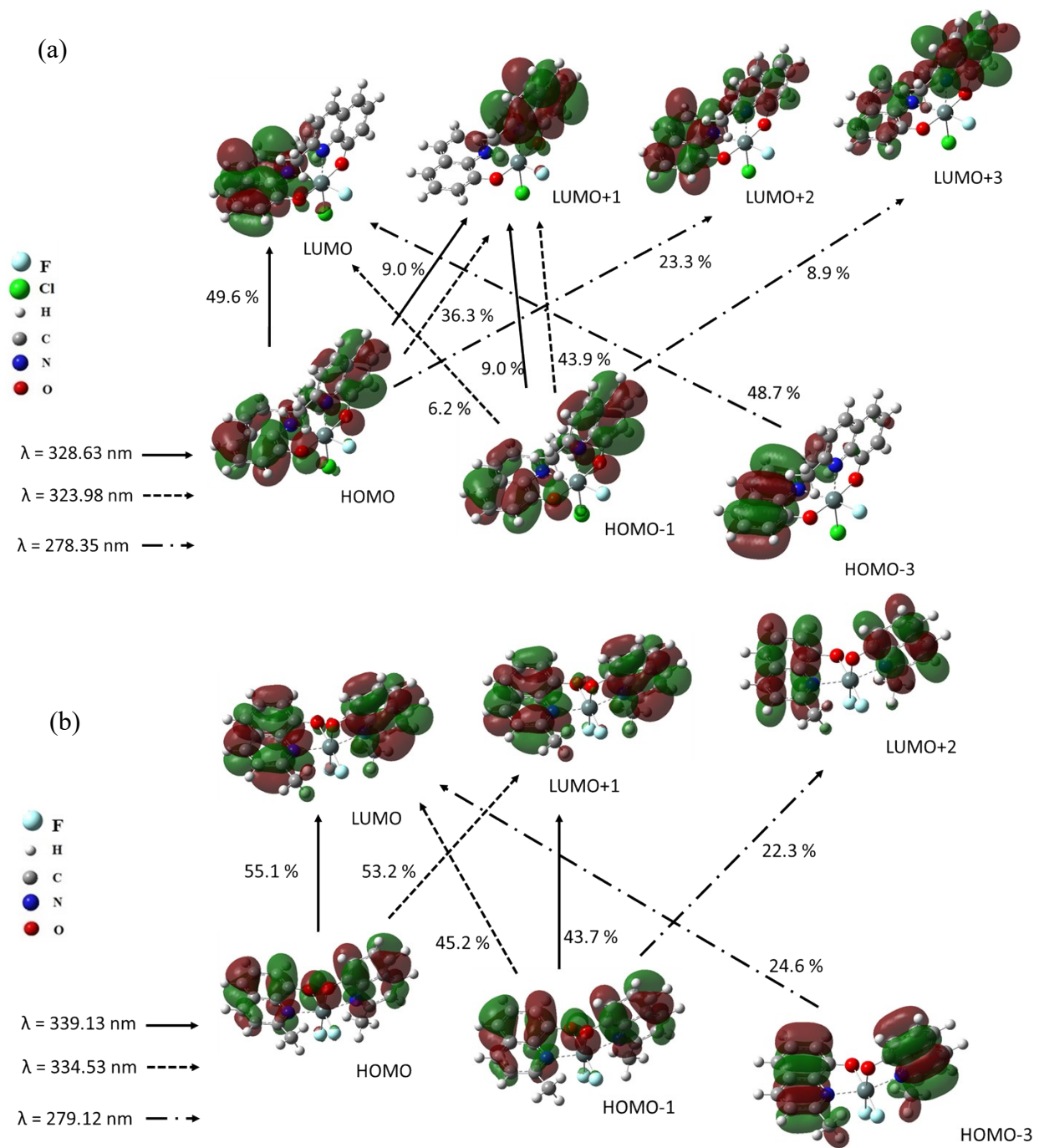


Figure S4. Calculated MO surfaces for complex **2** (a) and complex **3** (b)

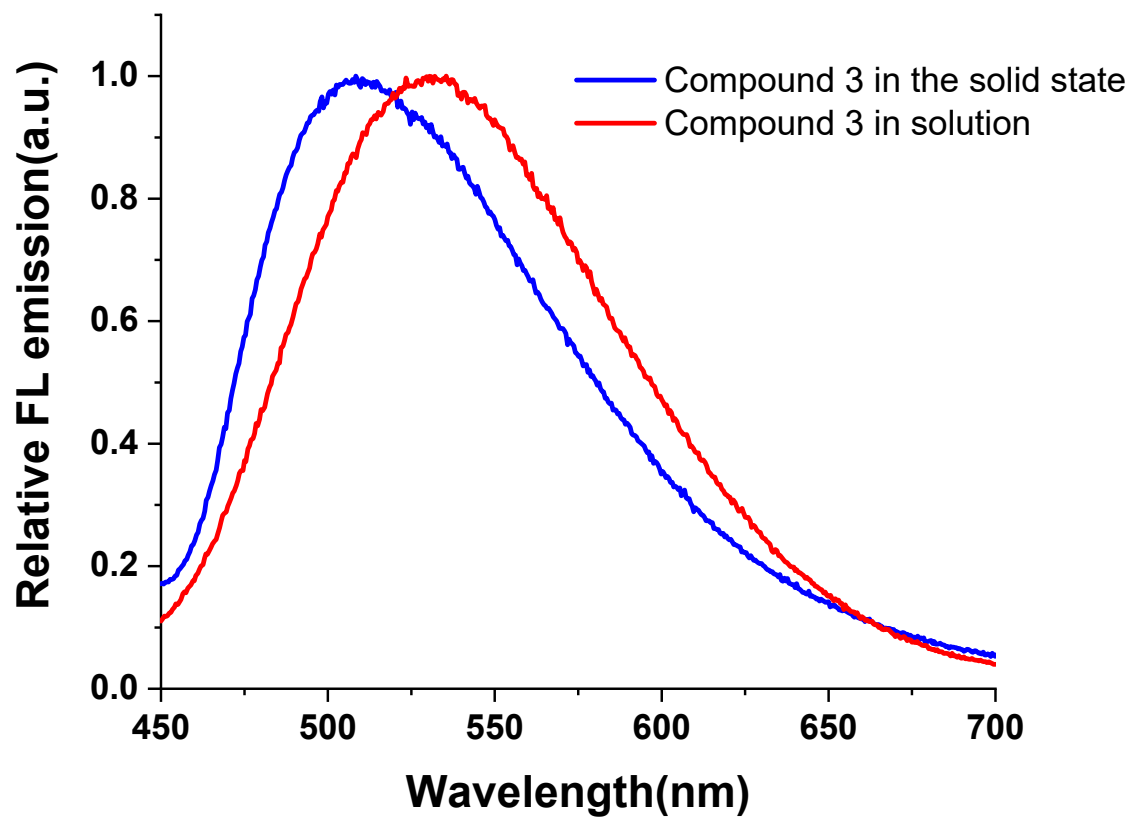


Figure S5. FL spectra of complex **3** in MeCN solution and crystalline solid state ( $\lambda_{ex}=360\text{nm}$ )

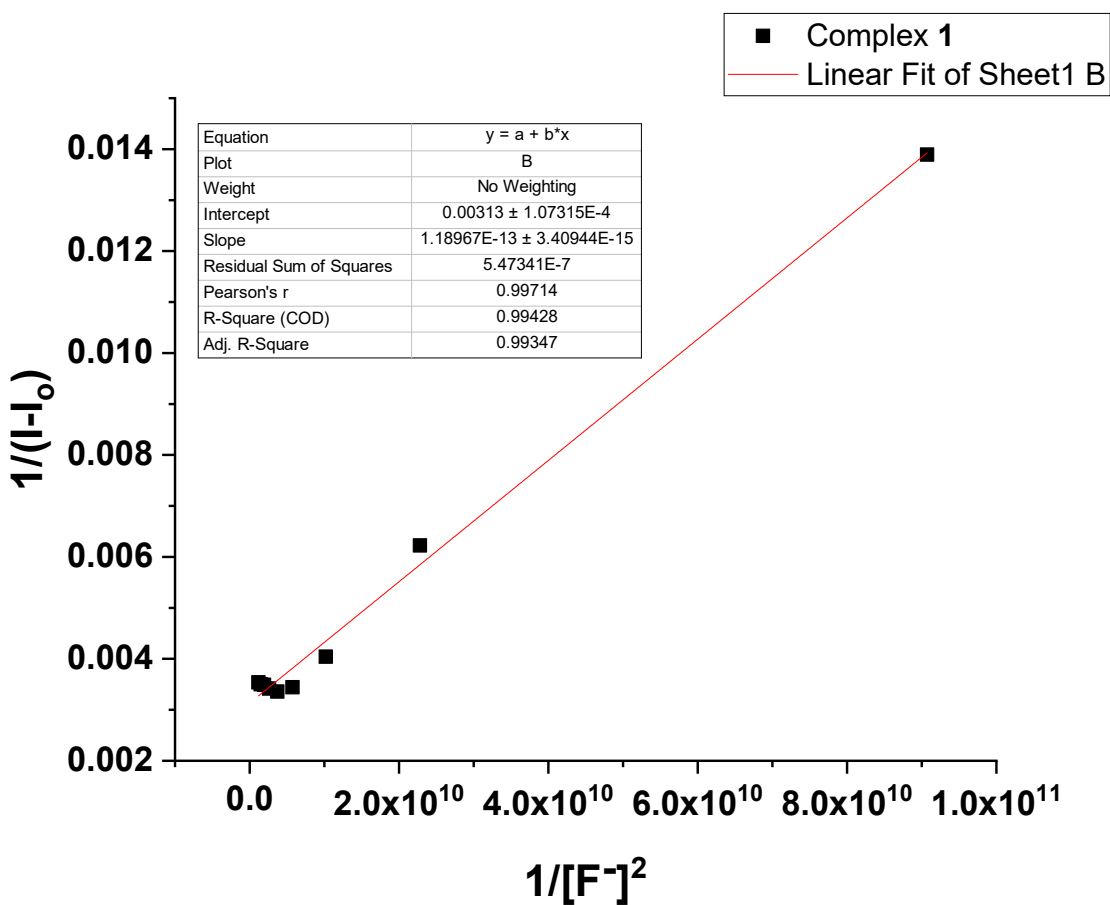


Figure S6. Benesi-Hildebrand plot using 1:2 stoichiometry (complex **1** and fluoride) for binding constant between complex **1** and fluoride ion. Benesi-Hildebrand equations is used by

$$\frac{1}{I - I_o} = \frac{1}{I' - I_o} + \frac{1}{(I' - I_o)K[F^-]^2}$$
 where  $I_o$  is FL intensity in the absence of  $F^-$ ,  $I$  is FL intensity at various concentration of  $F^-$  and  $I'$  is the max intensity in the presence of  $F^-$  ions.

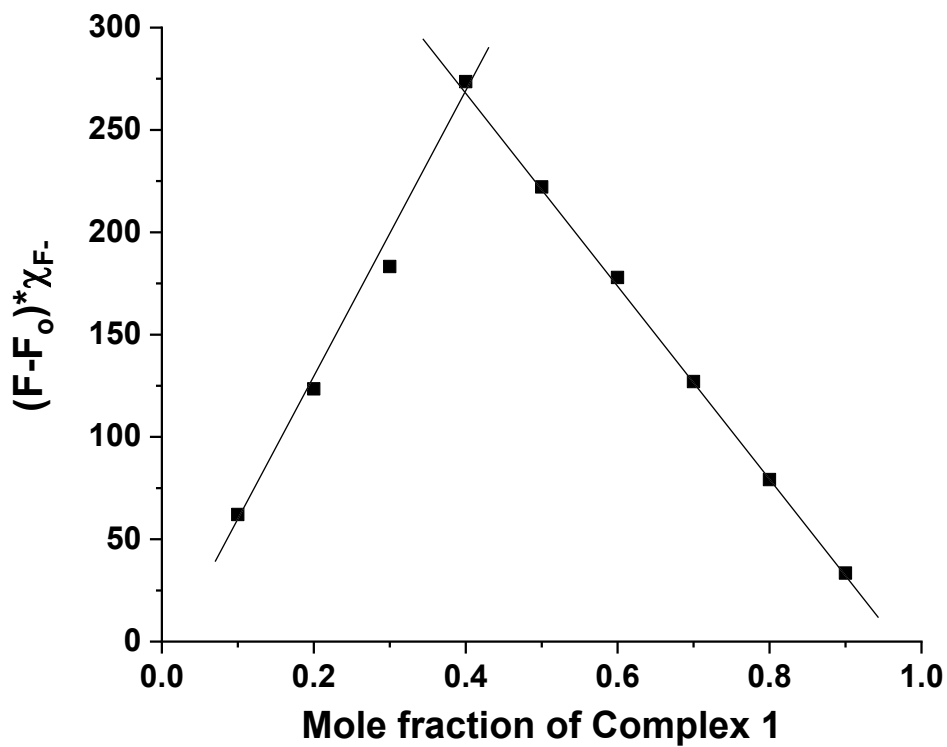


Figure S7. Job's plot for the determination of the stoichiometry of complex 1 and  $F^-$  in the MeCN.

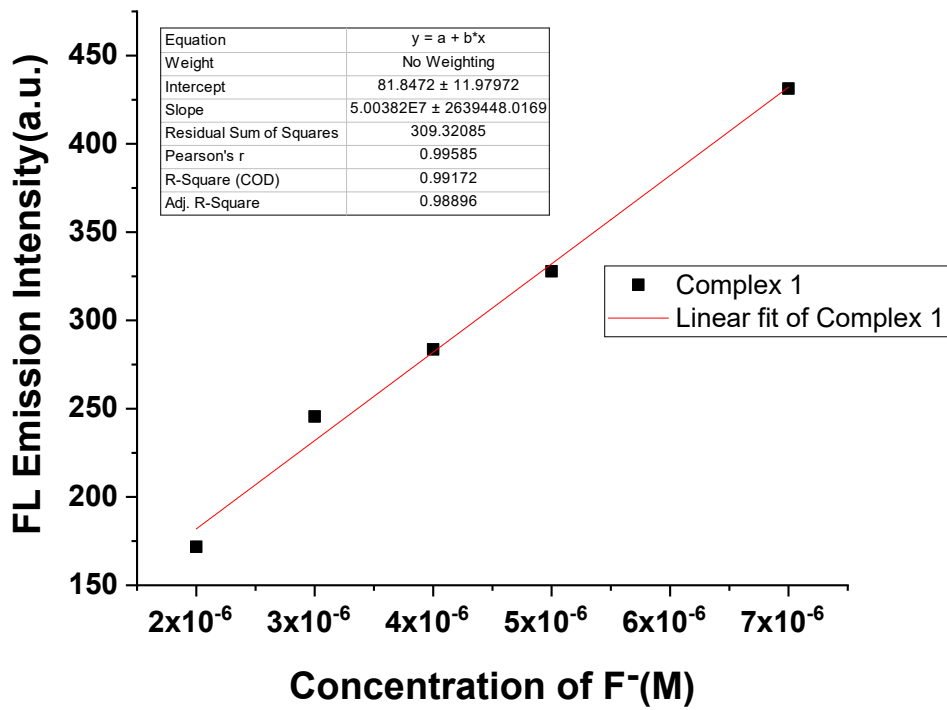


Figure S8. Fluorescence emission response of complex 1 against concentrations of fluoride ions to determine the limit of detection (LOD) obtained from the  $3\sigma/m$  ( $\sigma$ : the standard deviation of blank emission of complex 1 and  $m$ : the slope of calibration curve)

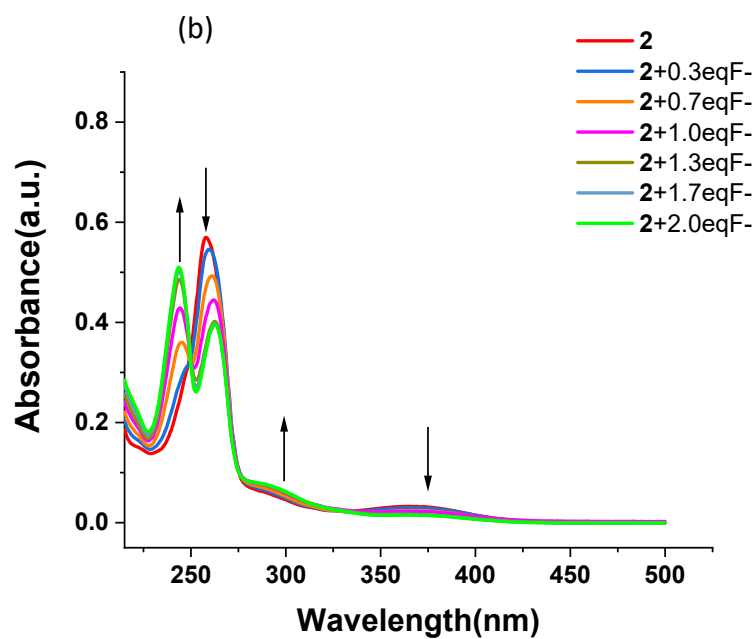
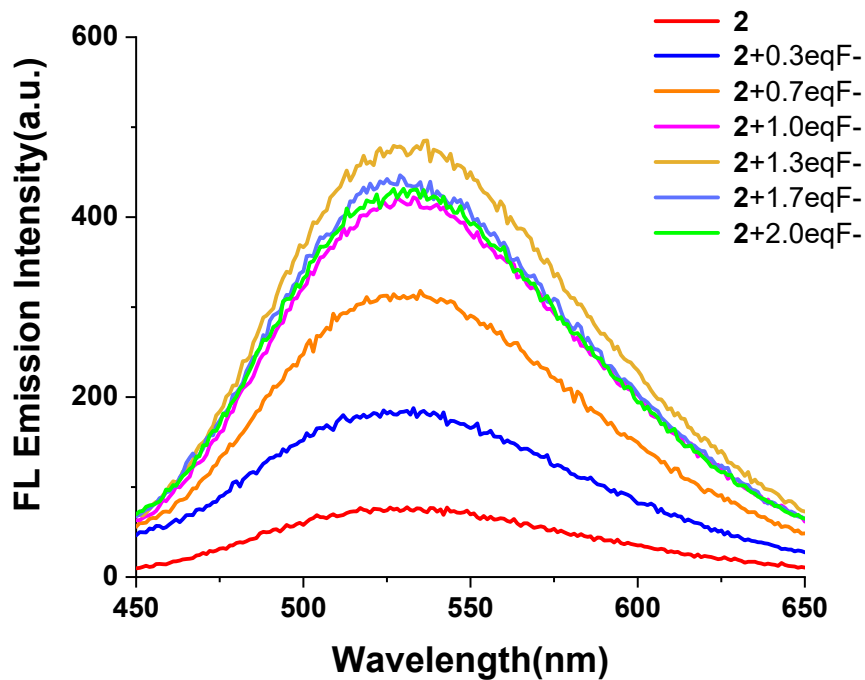


Figure S9. Fluorescence titration spectra(a) and UV-vis titration spectra (b) of complex **2** in MeCN solution upon the addition of F<sup>-</sup> from 0 to 2.0 eqv of F<sup>-</sup>

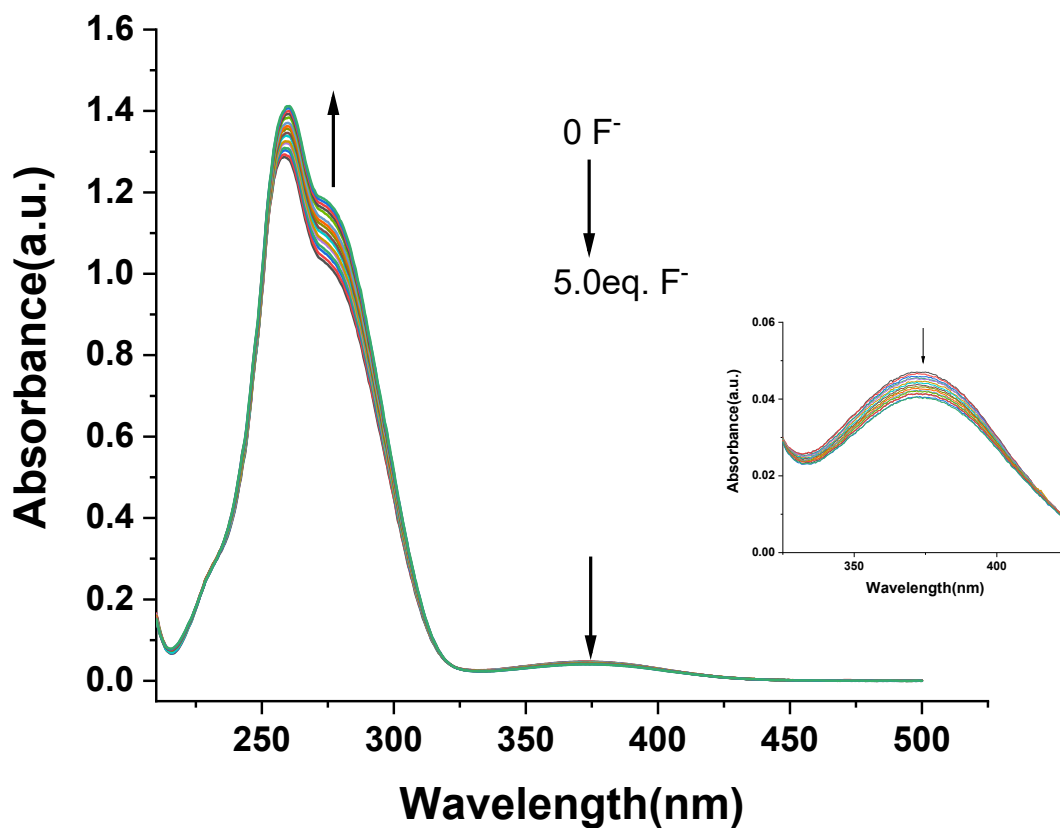


Figure S10. UV-Vis spectral changes upon the addition of tetrabutylammonium fluoride ( $1.0 \times 10^{-3}$  M in MeCN) in Snq<sub>2</sub>Cl<sub>2</sub> ( $1.0 \times 10^{-5}$  M in MeCN). Inset shows UV-Vis spectral changes at 375 nm

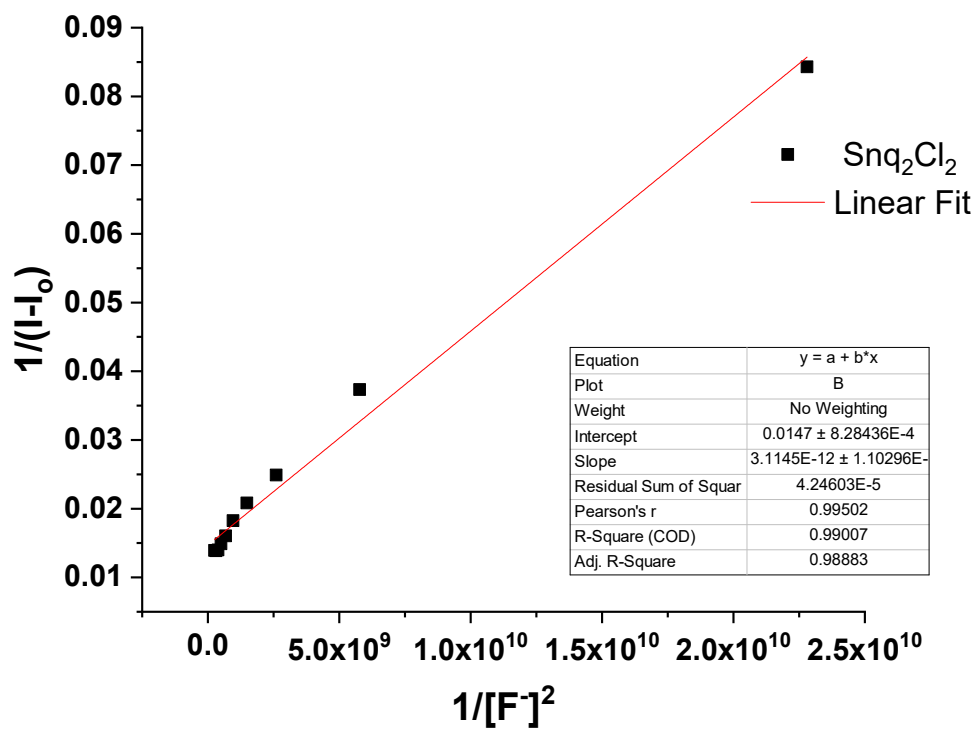


Figure S11. Benesi-Hildebrand plot using 1:2 stoichiometry(Snq<sub>2</sub>Cl<sub>2</sub> and fluoride) for binding constant between Snq<sub>2</sub>Cl<sub>2</sub> and fluoride ion.

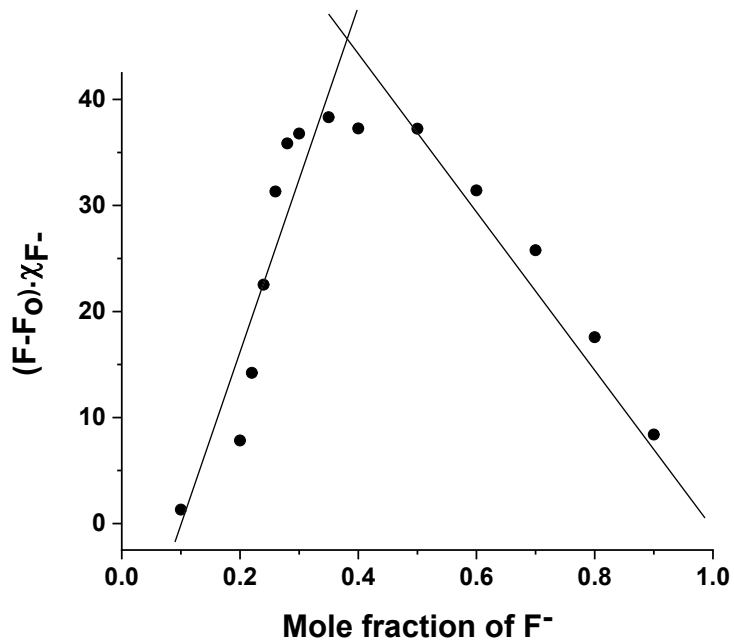


Figure S12. Job's plot for complex Snq<sub>2</sub>Cl<sub>2</sub>-fluoride interactions

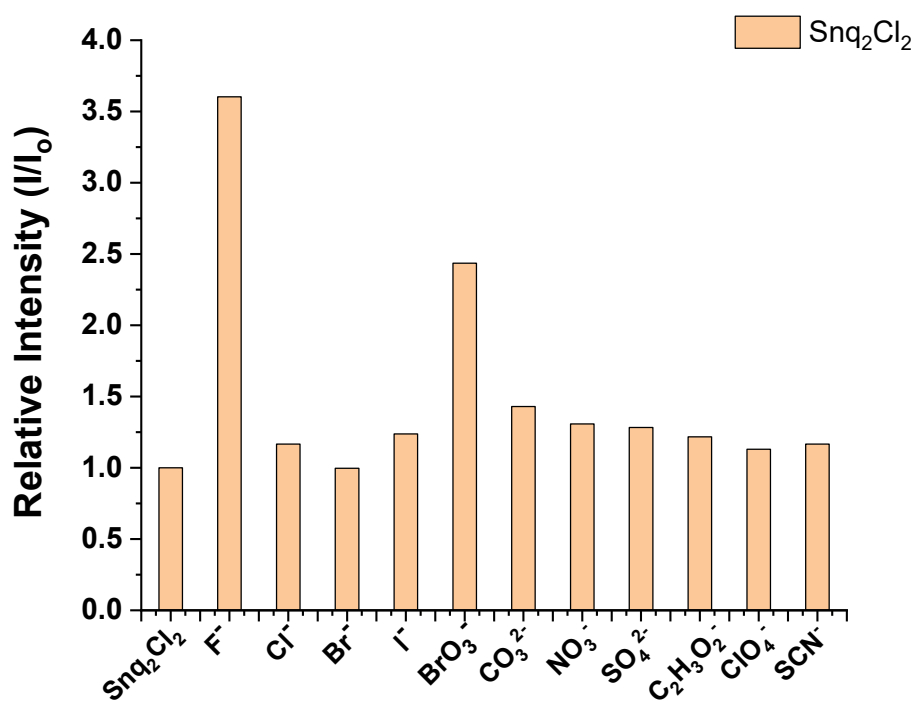


Figure S13. Emission intensity changes of Snq<sub>2</sub>Cl<sub>2</sub> in the presence of anions (2 equiv) in MeCN. Bars represent the ratio of emission intensity (I/I<sub>0</sub>), I<sub>0</sub> is the emission intensity of Snq<sub>2</sub>Cl<sub>2</sub> without anions at 530 nm.

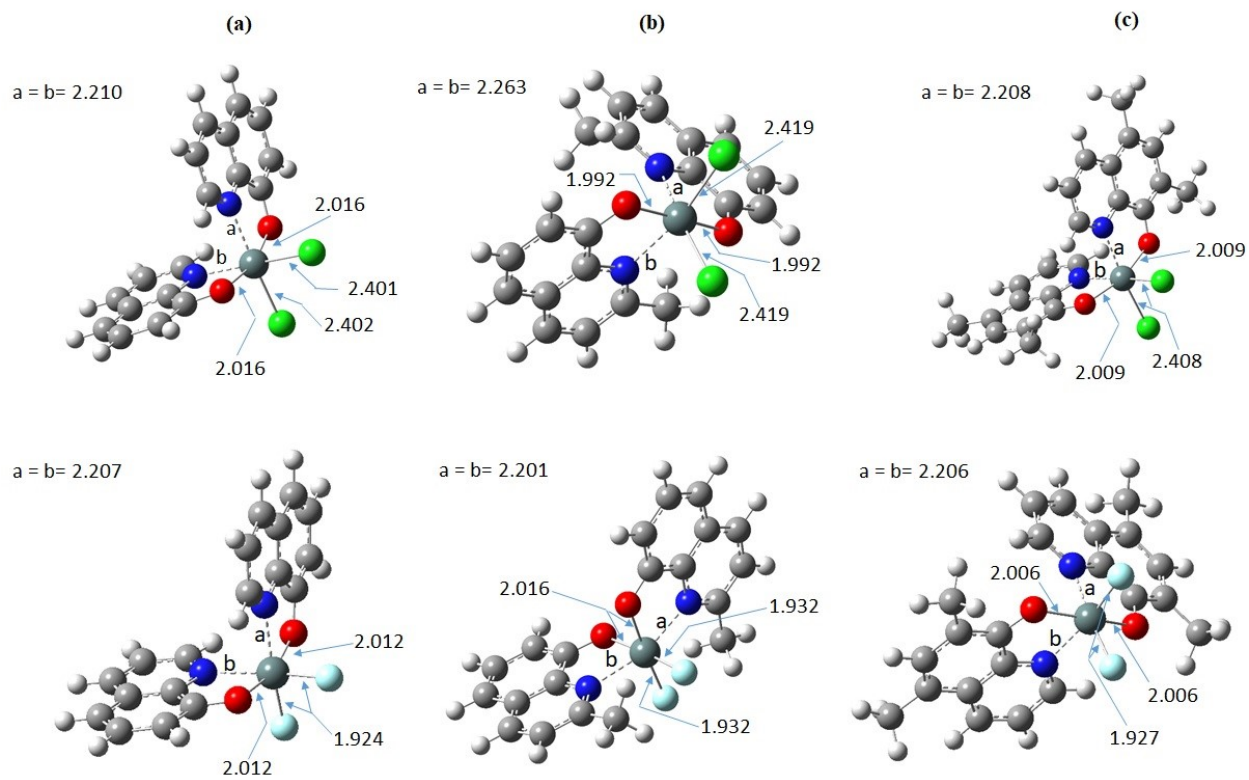


Figure S14. Optimized structure of  $\text{Snq}_2\text{Cl}_2$ ,  $\text{Sn}(\text{meq})_2\text{Cl}_2$ ,  $\text{Sn}(\text{dmqq})_2\text{Cl}_2$  and their respective fluorinated derivatives.